Received: 25 January 2019 | Revised: 10 June 2019 | Accepted: 9 September 2019 | Published on: 7 November 2019

DOI: 10.1002/met.1846

RESEARCH ARTICLE

Meteorological Applications RMetS

Numerical simulation of seasonal mesoscale atmospheric flow-field variables using ARW over the Singapore region: impact of land use land cover

Srikanth Madala[1] | **Santo V. Salinas**[1] | **Jukka Miettinen**[1] | **Jun Wang**[2,3]

[1]Centre for Remote Imaging Sensing and Processing, National University of Singapore, Singapore

[2]Center for Global and Regional Environmental Research, University of Iowa, Iowa City, Iowa, USA

[3]Department of Chemical and Biochemical Engineering, University of Iowa, Iowa City, Iowa, USA

Correspondence
Srikanth Madala, Research Scientist Centre for Remote Imaging, Sensing and Processing (ARW-CRISP) National University of Singapore (NUS), Singapore 119076.
Email: srikanthaesi@gmail.com, crssm@nus.edu.sg

Abstract

In the present study, the effect of land use land cover information on the simulation of seasonal planetary boundary layer (PBL) flow-field variables over the Singapore region is analysed using the Advanced Research Weather Research and Forecasting (ARW) mesoscale model. The results achieved are compared using the standard ARW Moderate Resolution Imaging Spectroradiometer (ARW-MODIS) global land cover data and a regional land cover map produced at the Centre for Remote Imaging, Sensing and Processing (ARW-CRISP), Singapore. The high-resolution simulations are conducted with triple-nested domains (horizontal grid spacing 27, 9 and 3 km) and 51 unequally spaced vertical sigma levels. The evolution of PBL variables and rainfall are modelled for four seasons (northeast monsoon season, first inter-monsoon period, southwest monsoon season and second inter-monsoon period). For the purpose of numerical simulations, 30 days in each season were considered and the model-simulated variables were validated with *in situ* available meteorological observations and rainfall at four stations over Singapore. The simulation results highlight the broad variation of the low-level flow-field in different seasons. The ARW mesoscale model simulated diurnal trends in surface meteorological variables and rainfall are in better agreement with observations by using the ARW-CRISP regional land cover map compared to ARW-MODIS global land cover data. Stronger winds are found during monsoon seasons compared with inter-monsoon periods. Overall, the results of the present study indicate that regional level air quality monitoring and prediction capabilities around Singapore can be improved by using up-to-date land cover products designed to take into account regional land cover characteristics.

KEYWORDS

ARW model, ARW-MODIS, land use land cover, planetary boundary layer

1 | INTRODUCTION

Southeast Asia (SEA) has experienced rapid developments over the past half century, leading to substantial environmental changes and deterioration of regional air quality. Accurate representation of meteorological fields and rainfall is important for air pollution monitoring to obtain accurate estimates of pollutant concentrations and enable short-term predictions. The planetary boundary layer (PBL) is the lowest region of the troposphere. Its vertical extent varies in

time and space, varying from hundreds of metres to a few kilometres (Stull, 1988). Numerical weather prediction (NWP) models generally have difficulties in calculating PBL flow-field variables and PBL height (Hu *et al*., 2010). Several recent studies have evaluated the performance of mesoscale models to predict the PBL flow-field variables with positive results (Garcia-Diez *et al*., 2013; Madala *et al*., 2015, 2017; Banks and Baldasano, 2016; Banks *et al*., 2016; Preeti and Manju, 2017).

Land surface plays an important role in regulating water and energy fluxes at the land and atmosphere interface. Land use land cover (LULC) characteristics influence soil moisture content and affect air temperature, PBL evolution, clouds and rainfall through the soil–moisture–evapotranspiration coupling, thereby affecting the transport and dispersion of air pollutants, air quality and atmospheric chemistry. Several recent studies have evaluated the effect of different LULC datasets on the Weather Research and Forecasting (WRF) model (Cheng *et al*., 2013; Tao *et al*., 2013; Rafee *et al*., 2015; Schicker *et al*., 2015; Yang and Duan, 2016). Tao *et al*. (2013) compared three land cover datasets in the USA (by the US Geological Survey [USGS], the University of Maryland and the Moderate Resolution Imaging Spectroradiometer [ARW-MODIS]) and found significant influence of land cover datasets on the assessment of some key atmospheric variables for air quality monitoring (e.g. PBL height and wind). Cheng *et al*. (2013), on the other hand, found that updated high-resolution (10 m) LULC information over Taiwan improved the estimation of wind speed and air temperature fields in particular, compared to the standard USGS land cover dataset available in the WRF model. Similarly, Schicker *et al*. (2015) achieved better results using high-resolution CORINE CLC06 land cover information in Austria. Finally, Yang and Duan (2016) noted that the use of an updated 2010 ARW-MODIS LULC dataset resulted in better performance of the WRF model in the northeastern Tibetan Plateau than an older (2001) version of the same product.

Relatively few studies exist on the performance of atmospheric mesoscale models in simulating surface meteorological variables and rainfall in the Singapore region (Li *et al*., 2013, 2016; Singh *et al*., 2015; Madala *et al*., 2019). Most recently, Madala *et al*. (2019) studied the effect of different PBL schemes, land cover datasets (USGS and MODIS) and different horizontal grid spacing by using the Advanced Research WRF (ARW) model for simulating the mesoscale flow-field variables over the Singapore region. They concluded that simulations using 3 km horizontal grid spacing with the MODIS LULC and with the asymmetric convective model (ACM2) PBL scheme most realistically represented surface meteorological variables over the Singapore region. Overall, these recent studies conducted both in the Singapore region and in other parts of the world have highlighted the considerable influence of land cover representation on the modelling of meteorological variables. From a land cover mapping point of view, the SEA archipelago is a very challenging environment. Although the proportion of primary forests in the region has dropped to less than half of the land area (Miettinen *et al*., 2016), over 80% of the landscape is still considered to be covered by woody vegetation (Hansen *et al*., 2013). Due to the extensively differing structural characteristics of primary rainforests and the various types of non-primary woody vegetation found in SEA, identification of the remaining primary forest areas is of high importance for numerical weather simulations. However, the standard land cover information available in the ARW model does not provide this distinction.

The principal objective of this present study was to analyse the impact of standard ARW-MODIS global LULC data and regional LULC data produced at the Centre for Remote Imaging, Sensing and Processing (ARW-CRISP) on the simulation of seasonal mesoscale atmospheric flow-field variables and rainfall over the Singapore region, for subsequent application in air pollution modelling and air quality studies.

2 | STUDY REGION

The study region for the present investigation comprises Singapore, an island city-state at the southern tip of the Malaysian Peninsula with a surface area of 700 km^2 (Figure 1). Singapore is a global economic focus point, with a tropical climate and a multicultural population of 5.6 million. It has an average elevation of 15 m above sea level, with the highest peak (Bukit Timah Hill) reaching 164 m. Singapore has a warm and humid climate all year round, with monthly average maximum and minimum temperatures 30–32°C and 24–25°C, respectively,

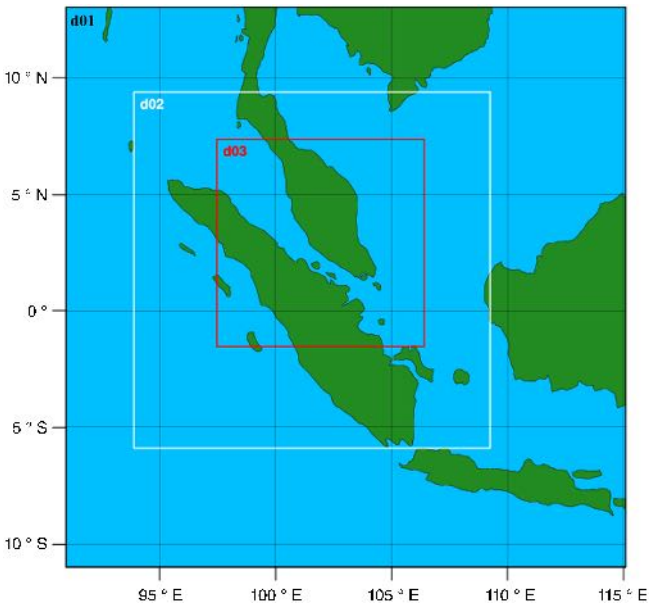

FIGURE 1 Domains used in the ARW model

and average monthly rainfall between 100 and 300 mm. In general, humidity does not vary much on a month-to-month basis and there is a uniform pattern throughout the year. The mean yearly relative humidity is around 84.0% (http://www.weather.gov.sg/climate-climate-of-singapore/).

In the present study, Singapore's annual climate cycle has been divided into four parts, as described by Chia and Foong (1991): northeast monsoon season (NEMS), first inter-monsoon period (FIMP), southwest monsoon season (SWMS) and second inter-monsoon period (SIMP). The NEMS occurs from December to early March and is characterized by north and northeastern winds. The SWMS, on the other hand, takes place during June to September and is characterized by south and southwestern winds. Singapore is more prone to haze episodes during this time of the year, due to the combination of wind direction and generally drier conditions regionally. The two inter-monsoon periods (FIMP from late March to May and SIMP from October to November) are characterized by lighter wind speed from variable directions.

3 | DATA AND METHODOLOGY

3.1 | Meteorological data

Surface meteorological observations of air temperature (AT) at 2 m, relative humidity (RH) at 2 m, wind speed (WS) at 10 m and wind direction (WD) at 10 m, obtained from four locations in Singapore at hourly intervals, are used for model validation. The observation data are taken from Iowa Environmental Mesonet (http://mesonet.agron.iastate.edu/request/download.phtml?network=KZ__ASOS) for the Changi (WSSS) (1.366 ° N, 103.983 ° E), Seletar (WSSL) (1.4166 ° N, 103.86 ° E) and Paya Lebar (WSAP) (1.36 ° N, 103.90 ° E) weather stations. In addition, an observation site within the National University of Singapore (NUS) (1.296 ° N, 103.776 ° E) is used (http://www.fas.nus.edu.sg/geog/weather/). Observation data quality checks used in the present study are given by Tyagi *et al*. (2012). Rainfall data for the above locations are obtained from the Meteorological Service, Singapore.

3.2 | Land cover data

The default LULC data for the ARW model is the global ARW-MODIS land cover dataset based on the international geosphere–biosphere programme (IGBP) classification (Figure 2a). This information is derived from a supervised classification of 2001 ARW-MODIS surface reflectance data and several auxiliary datasets derived at ~1 km spatial resolution (Friedl *et al*., 2002; Tao *et al*., 2013). Note that the IGBP class of "Evergreen broadleaf forest" includes all lands dominated by broadleaf woody vegetation with a canopy cover >60% and height above 2 m (Friedl *et al*., 2002). From this definition, nearly all the land area in our study domain is classified as "Evergreen broadleaf forest" class (Figure 2a).

The ARW-CRISP SEA regional map is based on 2015 ARW-MODIS surface reflectance data supported by auxiliary datasets. The mapping procedure starts with unsupervised clustering into 100 classes, followed by the assignment of 100 classes into six basic classes by visual image interpretation. Subsequently, the six basic classes were split into the final 19 classes (Figure 2b) with the help of the auxiliary datasets. The map was produced in 250 m spatial resolution. Full details of the mapping methodology are given by Miettinen *et al*. (2016). For the purposes of the present study, the ARW-CRISP map classes were reassigned

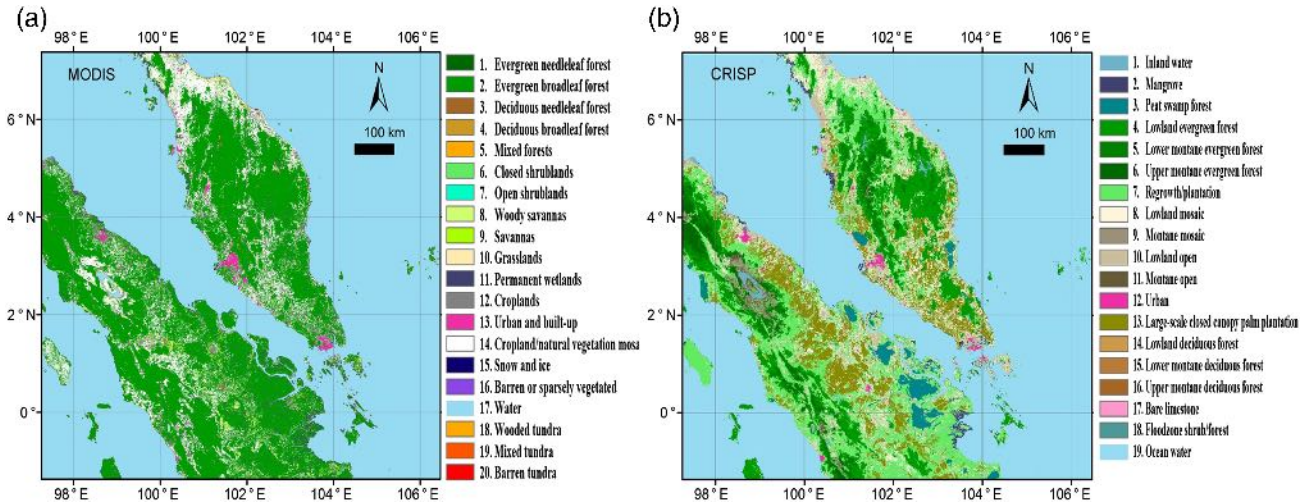

FIGURE 2 (a) ARW Moderate Resolution Imaging Spectroradiometer (ARW-MODIS) international geosphere–biosphere programme land cover and (b) Centre for Remote Imaging, Sensing and Processing (ARW-CRISP) land cover for ARW inner domain d03

TABLE 1 Class conversion from CRISP land cover classes to USGS-24 land cover classes

	CRISP		USGS-24
Code	Name	Code	Name
1	Water	16	Water bodies
2	Mangrove	18	Wooden wetland
3	Peat swamp forest	18	Wooden wetland
4	Lowland evergreen forest	13	Evergreen broadleaf forest
5	Lower montane evergreen forest	13	Evergreen broadleaf forest
6	Upper montane evergreen forest	13	Evergreen broadleaf forest
7	Regrowth/ plantation	8	Shrubland
8	Lowland mosaic	6	Cropland/woodland mosaic
9	Montane mosaic	6	Cropland/woodland mosaic
10	Lowland open	4	Mixed dryland/irrigated cropland and pasture
11	Montane open	2	Dryland cropland and pasture
12	Urban	1	Urban and built-up land
13	Large-scale closed canopy palm Plantation	8	Shrubland
14	Lowland deciduous forest	11	Deciduous broadleaf forest
15	Lower montane deciduous forest	11	Deciduous broadleaf forest
18	Flood zone shrub/ forest	8	Shrubland
19	Ocean water	16	Water bodies

into the USGS-24 land use categories, for which necessary variables are available within ARW (Cheng *et al*., 2013; Schicker *et al*., 2015) (Table 1).

3.3 | Model simulation period

The study aim was to compare the performance of ARW-MODIS and ARW-CRISP LULC datasets using the ARW model over the Singapore region in the four different seasons described in Section 2. For the purpose of numerical simulations, 30 days (1 month) in each season were considered. The selected dates for simulations are January 15 to February 14, 2015, for NEMS; April 15 to May 15, 2015, for FIMP; July 15 to August 14, 2015, for SWMS; and October 15 to November 14, 2015, for SIMP.

3.4 | Model configuration and initialization

The ARW mesoscale model (version 3.8) (Skamarock *et al*., 2008) was used to simulate the seasonal mesoscale atmospheric flow-field variables in the Singapore region. The ARW mesoscale model considers three nested horizontal grid spacings (27, 9 and 3 km) and 51 unequally spaced vertical sigma levels with the model top at 50 hPa (Figure 1). The second and third nested domains are two-way interactive. The ARW model is initialized at 1200 UTC and integrated for a period of 132 hr (5.5 days) for all simulations and the first 12 hr (half day) are considered ARW model spin up in each simulation. The model simulations start at January 14, 19, 24, 29, February 3 and 8, 2015, for NEMS, April 14, 19, 24, 29, May 4 and 9, 2015, for FIMP, July 14, 19, 24, 29, August 3 and 8, 2015, for SWMS, and October 14, 19, 24, 29, November 3 and 8, 2015, for SIMP. The ARW model is run with 6 hr National Centre for Environmental Prediction (NCEP) final analysis (FNL) data with $1.0° \times 1.0°$ for the initial and boundary conditions. The ARW model configurations used in the present study are based on the results obtained in an earlier study in the same study region by Madala *et al*. (2019) (Table 2).

3.5 | ARW model validation and statistical assessment

The ARW model-simulated surface meteorological variables (AT and RH at 2 m as well as WS and WD at 10 m) and rainfall during the study period are validated with available observations. The ARW model simulations are evaluated both qualitatively and quantitatively over the study region. Statistical error statistics of mean bias (MB), mean absolute error (MAE), root mean square error (RMSE) and correlation co-efficient (CC) are estimated between model outputs and observations.

4 | RESULTS AND DISCUSSION

4.1 | Surface meteorological variables

In this section, the relative performance of ARW-MODIS and ARW-CRISP LULC datasets in simulating the diurnal variation of the surface meteorological variables (AT, RH, WS and WD) using ARW is evaluated with hourly *in situ* available observations at the NUS, WSAP, WSSL and WSSS. The diurnal variations of AT at 2 m and RH at 2 m simulated with ARW-MODIS and ARW-CRISP datasets are depicted in Figures 3 and 4 along with available observations from January 15 to February 14, 2015, for the NEMS at NUS, WSAP, WSSL and WSSS. Statistical analysis was performed to quantify the model errors for simulation of the various variables. The errors (MB, MAE, RMSE and CC)

TABLE 2 Overview of ARW model configuration over Singapore

Dynamics	Non-hydrostatic
Initial and boundary data	NCEP FNL
Temporal interval of boundary data	6 hr
Grid size	Domain 1: (100 × 100) × 51 Domain 2: (190 × 190) × 51 Domain 3: (331 × 331) × 51
Resolution	Domain 1: 27 × 27 km Domain 2: 9 × 9 km Domain 3: 3 × 3 km
Map projection	Mercator
Horizontal grid system	Arakawa-C grid
Integration time step for outermost domain	90 s
Vertical co-ordinates	51 vertical levels
Time integration scheme	3rd order Runge–Kutta scheme
Spatial differencing scheme	6th order centre differencing
PBL schemes	Asymmetric convective model (ACM2)
Cumulus parameterization	Kain–Fritsch scheme (only for d01and d02)
Surface layer parameterization	Noah land surface scheme
Microphysics	Goddard microphysics scheme
Short wave radiation	Dudhia scheme
Long wave radiation	RRTM scheme
Terrain and land use data	MODIS and CRISP

calculated between the model simulated and observed surface meteorological variables for NEMS for the combination of all four observation stations are shown in Table 3.

In general, it can be seen that the ARW-MODIS and ARW-CRISP datasets simulated the diurnal variation of AT and RH realistically at all stations for the NEMS except the NUS. The observed mean AT in Singapore (average of the four stations) for the NEMS is 26.8°C; a slight cold bias with ARW-MODIS, a warm bias with ARW-CRISP and around 5.5°C variation in day and night temperatures are noticed (Figure 3a–d). Both datasets slightly overpredicted AT at the NUS; underprediction is noticed at the other three stations during the day time. The ARW-MODIS simulated a slight cold bias, model – observations <0, in the night time, but a warm bias was seen in the simulations based on the ARW-CRISP dataset at the NUS station for the NEMS and both datasets closely simulated night time AT for the other three stations. For AT, both datasets give fewer errors and good correlations for the NEMS, but a slightly better performance is noticed with ARW-MODIS. It can also be seen in Figure 4a–d that both day time and night time RH is generally underestimated with the ARW-CRISP dataset, particularly at the NUS site, while the ARW-MODIS dataset tends to overestimate night time RH. The observed mean RH is around 73.2%, indicating a slightly positive mean bias in RH with ARW-MODIS and a negative mean bias with ARW-CRISP in the NEMS. For RH, a relatively smaller error and good correlations are noticed from ARW-CRISP compared to ARW-MODIS for the NEMS (Table 3).

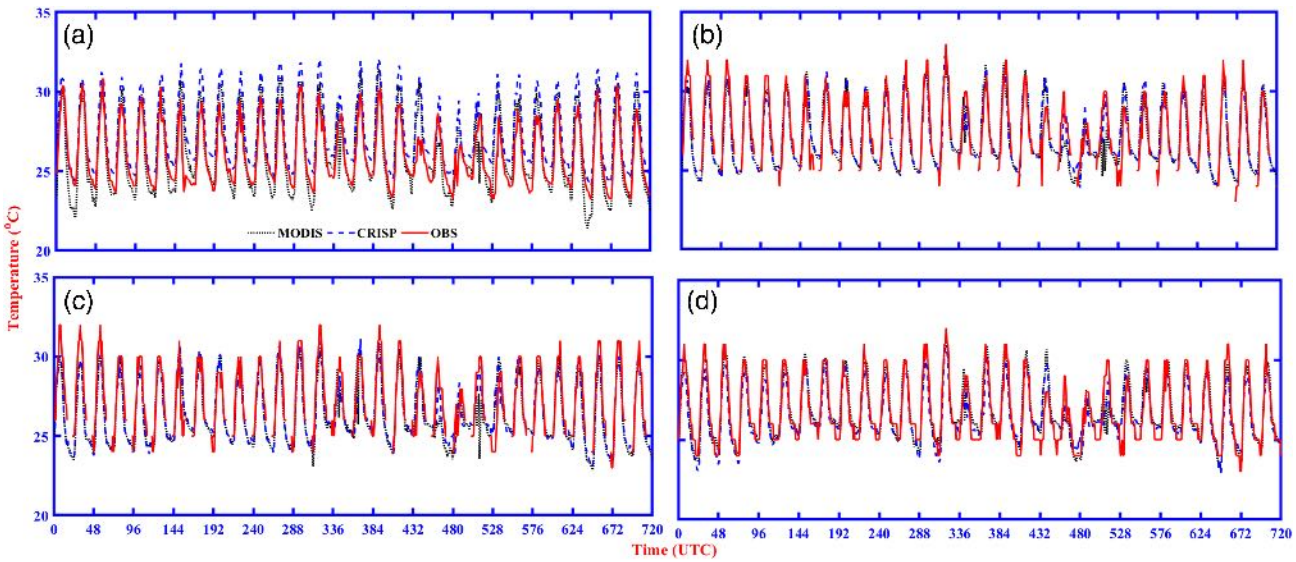

FIGURE 3 Validation of ARW model simulations of air temperature at 2 m during January 15 to February 14, 2015, at (a) the National University of Singapore, (b) Paya Lebar (WSAP), (c) Seletar (WSSL) and (d) Changi (WSSS) for the northeast monsoon season

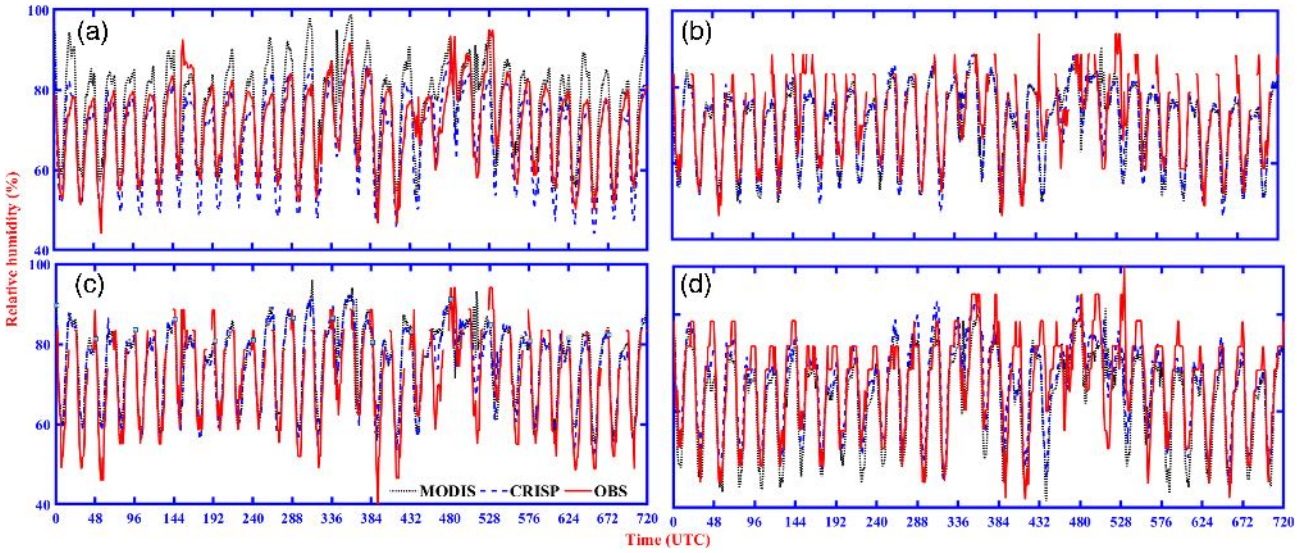

FIGURE 4 Validation of ARW model simulations of relative humidity at 2 m during January 15 to February 14, 2015, at (a) the National University of Singapore, (b) Paya Lebar (WSAP), (c) Seletar (WSSL) and (d) Changi (WSSS) for the northeast monsoon season

TABLE 3 Statistical examination of surface meteorological parameters with MODIS, CRISP for northeast monsoon season

	Air temperature (°C) (N = 2,576)		Relative humidity (%) (N = 2,581)		Wind speed (ms^{-1}) (N = 2,510)		Wind direction (°) (N = 2,558)	
	MODIS	CRISP	MODIS	CRISP	MODIS	CRISP	MODIS	CRISP
MB	−0.06	0.20	0.09	−1.07	−0.14	0.33	−13.84	−11.54
MAE	0.74	0.87	5.66	4.75	1.55	1.56	21.23	19.16
RMSE	1.01	1.12	7.41	6.28	1.93	1.92	83.27	80.98
CC	0.89	0.86	0.76	0.83	0.40	0.47	0.69	0.70

The WS and WD evaluations were made through joint frequency distribution figures (wind roses). The wind roses for WS and WD from the ARW model and available observations are presented for the NEMS in Figure 5, and statistical analyses are shown in Table 3. The average observed WS is around 5.17 ms^{-1} over Singapore for the NEMS. In general, the winds are predominantly northeasterly and northnortheasterly. Both datasets captured the speed and directions reasonably well. However, a slight overestimation of WS is found for the ARW-CRISP dataset and underestimation is noticed for ARW-MODIS dataset for the NEMS. The ARW-CRISP dataset produces better results for both WS and WD simulations (Table 3).

For FIMP (April 15 to May 15, 2015), for both datasets the simulated diurnal variation of AT is underestimated (Table 4). In particular at the NUS site, both datasets overestimated AT in both day and night time. All other stations are well simulated for the diurnal variation of AT (Figure S1). The observed AT of Singapore for the FIMP is 28.8°C and the variation of day and night AT is around 9.0°C. The higher day and night variations, together with larger day time heating, enable stronger convective mixing of air pollution in the FIMP than in other seasons. The observed mean RH is around 77.0%. A positive mean bias in RH was observed with the ARW-MODIS simulation, while the ARW-CRISP simulation resulted in a slight negative mean bias (Table 4). Compared to day time RH (around 55%), night time RH (about 90%) is well captured with both dataset simulations (Figure S2). In the case of ARW-MODIS simulations, some overprediction is noticed in the day time compared to the night time RH.

The wind rose plot for the FIMP shows considerable directional variability, with WD predominantly from northeasterly, north, northwesterly, south, southeasterly and less predominantly from western sectors (Figure 6). The average observed WS is around 2.56 ms^{-1}. The WS is well predicted by both ARW-MODIS and ARW-CRISP simulations, but a slight deviation is noticed for WD. Large variations in WD would lead to shifting in the plume dispersion direction in air quality studies (Table 4).

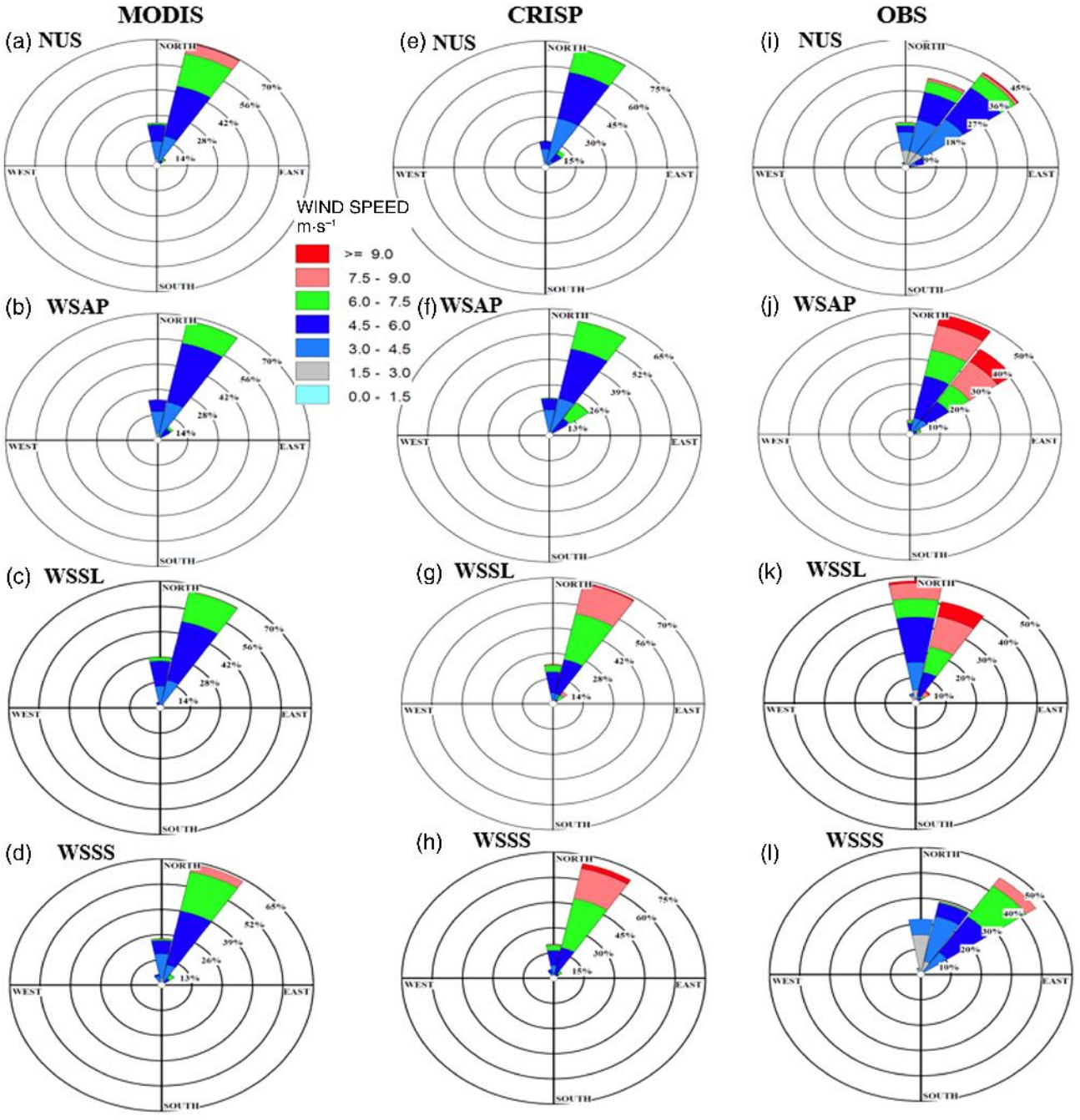

FIGURE 5 Wind roses at 10 m during January 15 to February 14, 2015, for the northeast monsoon season with observations

TABLE 4 Statistical examination of surface meteorological parameters with MODIS, CRISP for the first inter-monsoon period

	Air temperature (°C) (N = 2,480)		Relative humidity (%) (N = 2,528)		Wind speed (ms^{-1}) (N = 2,362)		Wind direction (°) (N = 2,081)	
	MODIS	**CRISP**	**MODIS**	**CRISP**	**MODIS**	**CRISP**	**MODIS**	**CRISP**
MB	−0.30	−0.07	0.77	−0.68	0.14	0.13	6.89	−6.11
MAE	1.25	1.23	7.45	6.79	1.28	1.21	71.88	63.77
RMSE	1.65	1.63	9.53	8.89	1.68	1.57	110.01	99.22
CC	0.73	0.72	0.64	0.69	0.32	0.43	0.46	0.56

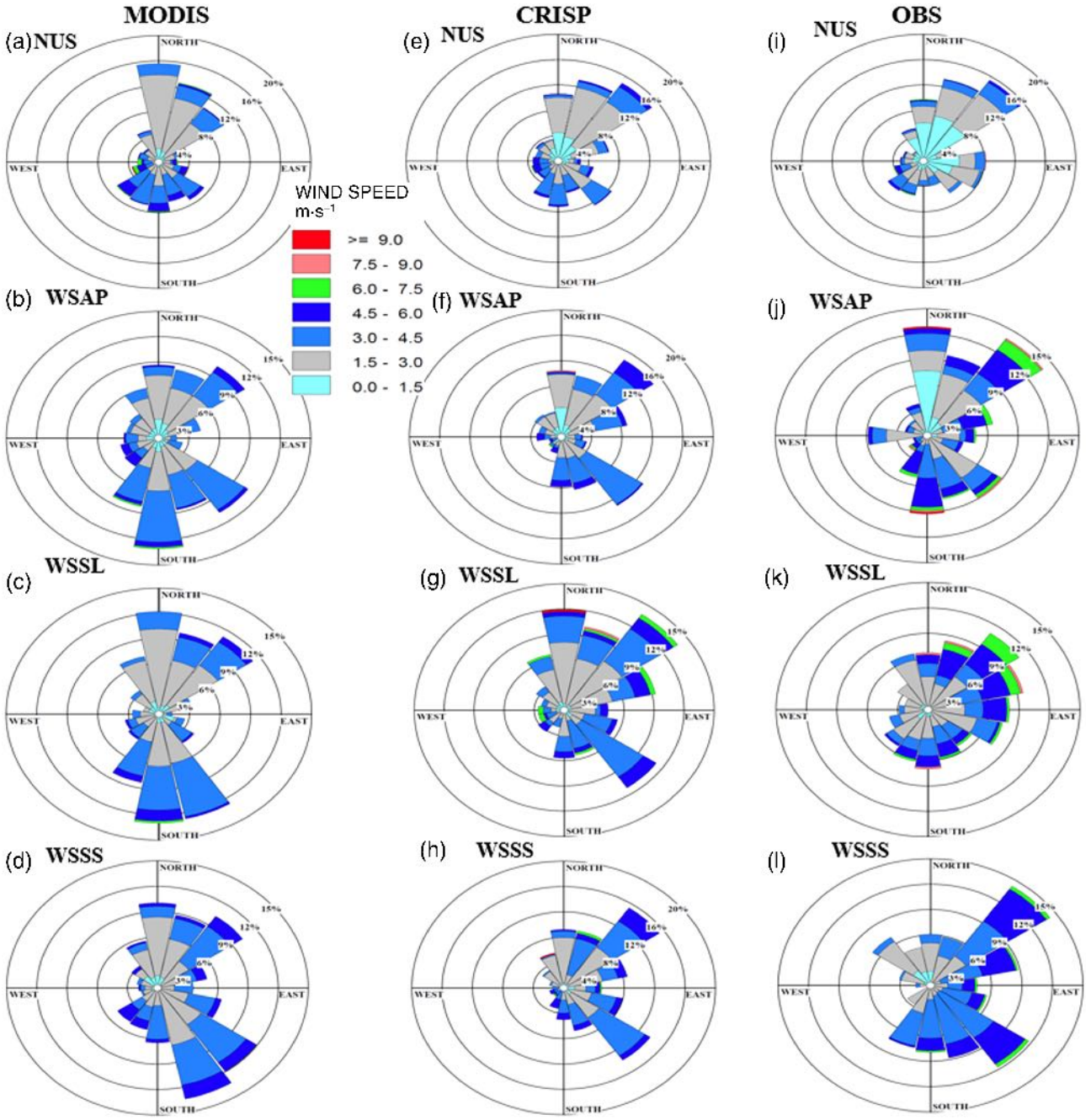

FIGURE 6 Wind roses at 10 m during April 15 to May 15, 2015, for the first inter-monsoon period with observations

TABLE 5 Statistical examination of surface meteorological parameters with MODIS, CRISP for the southwest monsoon season

	Air temperature (°C) (N = 2,578)		Relative humidity (%) (N = 2,578)		Wind speed (ms^{-1}) (N = 2,512)		Wind direction (°) (N = 2,383)	
	MODIS	CRISP	MODIS	CRISP	MODIS	CRISP	MODIS	CRISP
MB	−0.11	0.03	0.67	−0.25	0.46	0.20	11.57	3.63
MAE	1.17	1.21	7.36	6.70	1.48	1.23	39.93	35.77
RMSE	1.55	1.61	9.60	8.91	1.86	1.57	58.60	52.79
CC	0.64	0.62	0.50	0.58	0.24	0.46	0.22	0.37

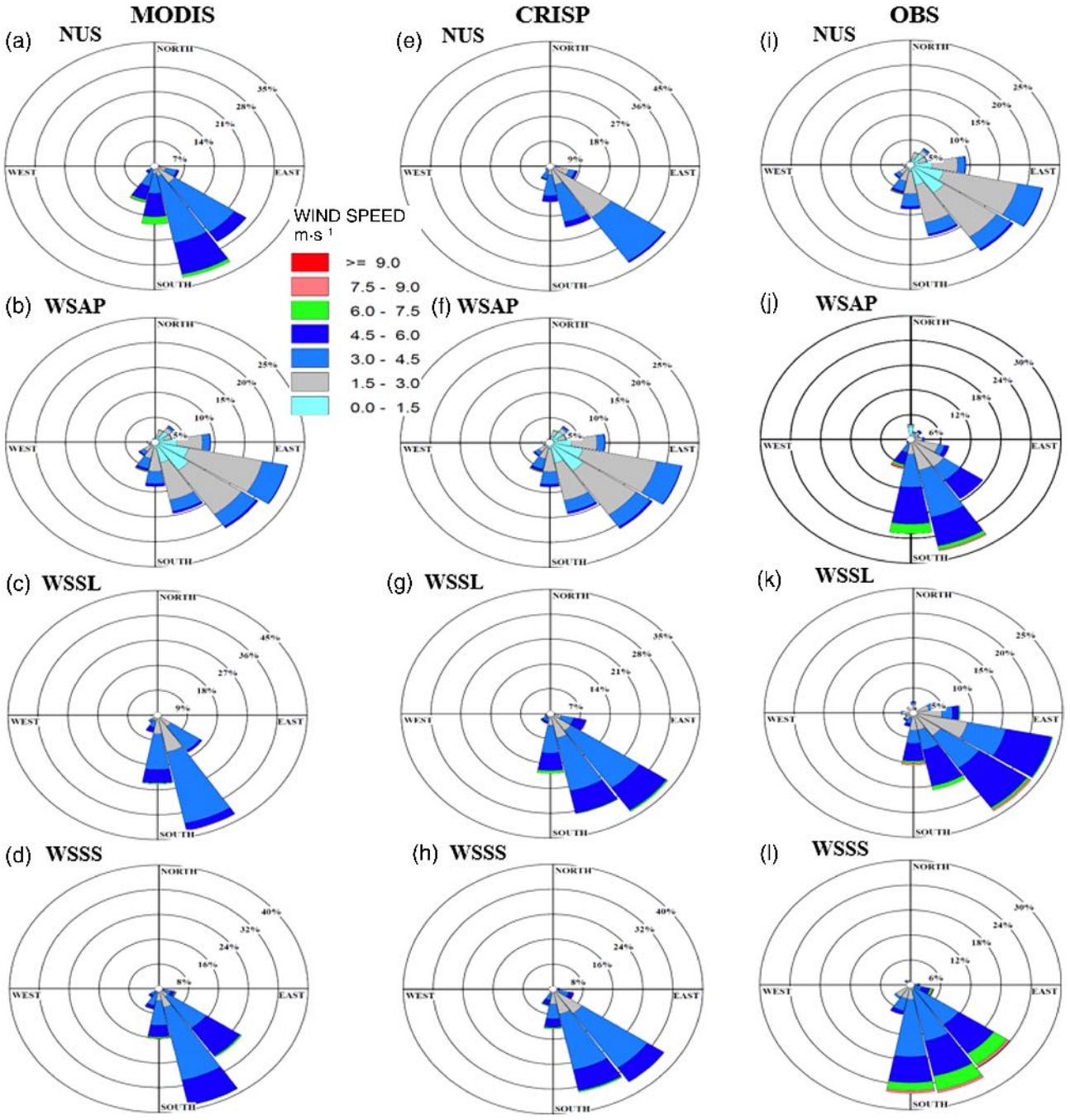

FIGURE 7 Wind roses at 10 m during July 15 to August 14, 2015, for the southwest monsoon season with observations

The diurnal variations of AT and RH for the SWMS (Figure S3) show that both of the LULC datasets result in reasonably well simulated diurnal cycles of thermodynamic variables during this season. The mean observed AT during the period is 28.65°C and the variation of day and night AT is around 6.5°C (Table 5). Both datasets underpredict day time AT for all stations except in the NUS, while simulations with the ARW-MODIS dataset show slight AT deviations during both day time and night time. More cold bias is noticed for AT with the ARW-MODIS dataset compared to the ARW-CRISP dataset during night time, particularly at the NUS site. RH is overestimated during the day time but better simulated during night time with both datasets (Figure S4). The observed mean humidity for the SWMS is around 75.1%. A light humid bias is noticed in the ARW-MODIS simulation and a dry bias in the ARW-CRISP simulation during the SWMS (Table 5).

TABLE 6 Statistical examination of surface meteorological parameters with MODIS, CRISP for the second inter-monsoon period

	Air temperature (°C) (N = 2,568)		Relative humidity (%) (N = 2,568)		Wind speed (ms^{-1}) (N = 2,428)		Wind direction (°) (N = 2,177)	
	MODIS	CRISP	MODIS	CRISP	MODIS	CRISP	MODIS	CRISP
MB	−0.17	0.22	−0.56	−2.70	0.19	0.20	14.85	−3.58
MAE	1.20	1.21	8.06	7.36	1.16	1.13	75.20	67.81
RMSE	1.57	1.62	10.17	9.65	1.50	1.46	108.67	98.09
CC	0.72	0.70	0.64	0.70	0.37	0.43	0.35	0.43

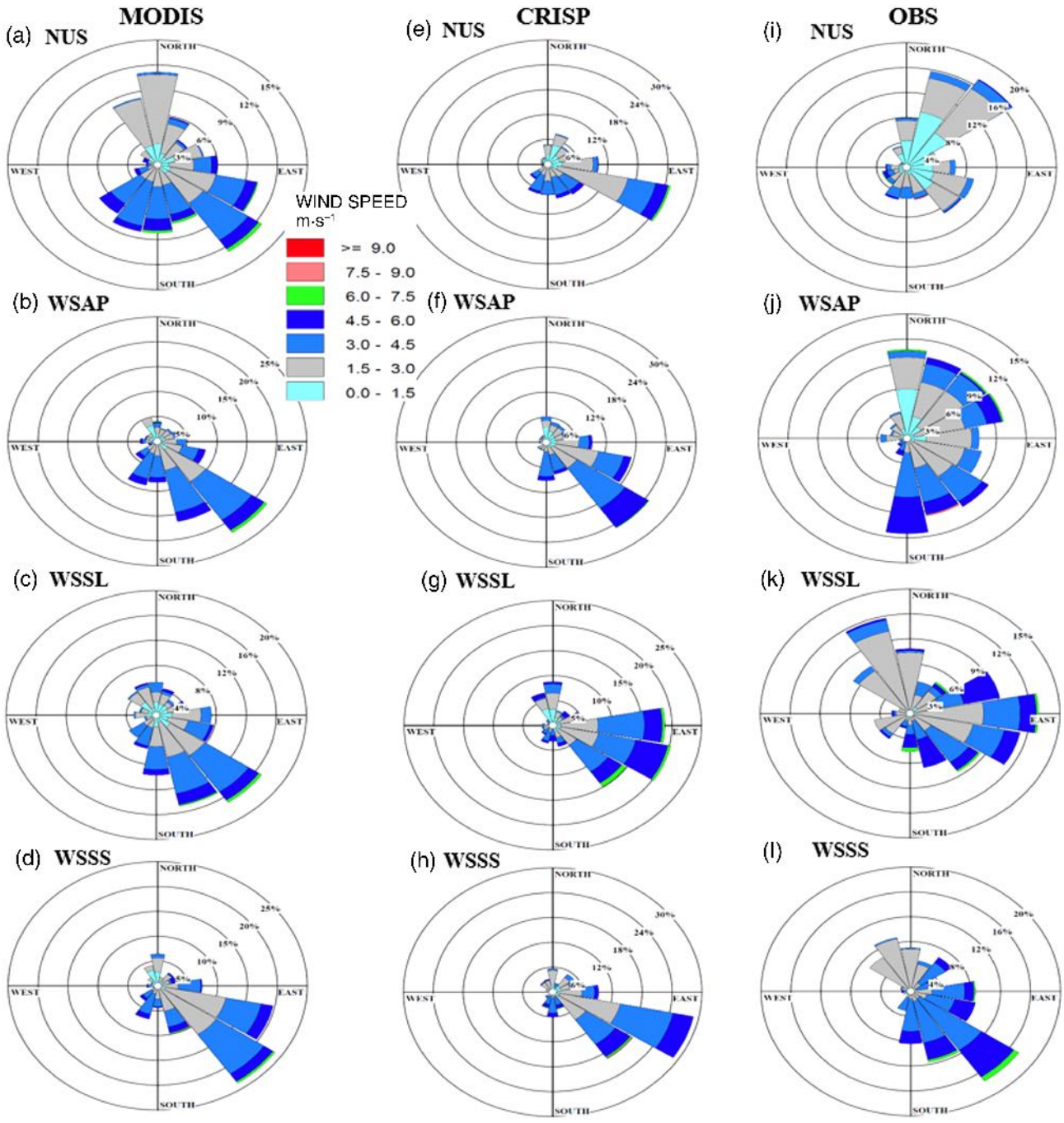

FIGURE 8 Wind roses at 10 m during October 15 to November 14, 2015, for the second inter-monsoon period with observations

Wind roses from the models and observations are presented in Figure 7. The wind flow is predominantly southeasterly, the southeast sector followed by the southwest sector during the SWMS over the Singapore region. This flow pattern is well simulated with the ARW-CRISP dataset, including both WS and WD (Table 5). The average observed WS is around 3.16 ms^{-1}. Both datasets overestimate the winds. WD deviations are noted in the results obtained with the ARW-MODIS dataset. However, both (ARW-MODIS and ARW-CRISP) datasets fail to capture the south and southwest sector winds in the SWMS (Figure 7).

The diurnal variation of AT and RH simulated with the ARW-MODIS and ARW-CRISP datasets along with the available observations for SIMP (Figures S5 and S6) show significant day time warm bias for the ARW-CRISP simulation and a night time cold bias for the ARW-MODIS simulation at the NUS site. In general, one can see that both datasets simulate the diurnal variation of AT reasonably well, as seen in the observations for the other three stations (WSAP, WSSL and WSSS). The mean observed AT during the SIMP is 28.7°C, and the variability of day and night AT is around 7.0°C (Table 6). In the case of RH at the NUS site, the ARW-MODIS simulation results in considerable overprediction at night time, while the ARW-CRISP simulation results in underprediction at day time. The observed mean humidity for the SIMP is around 74%. More errors are noticed in the results based on the ARW-MODIS dataset for RH in the SIMP (Table 6). Wind roses for the SIMP are presented in Figure 8. Unlike other seasons, the WD in the SIMP was noticed in the northeasterly, north, northwesterly sectors and southeasterly sectors. While WS is well captured with both datasets, a slight overprediction is noticed and WD is not captured well. Higher errors are noticed for WD compared to the other seasons. However, compared to the ARW-MODIS simulation, less error is noticed when using the ARW-CRISP dataset for both WS and WD in the SIMP (Table 6). WD deviations might be due to improper calculation of surface drag co-efficients by the surface layer schemes, which needs further analysis and modification of the corresponding drag variables. Overall, both the ARW-MODIS and ARW-CRISP datasets result in poor simulations of WD during the SIMP.

From the qualitative and quantitative analyses of the results presented above, it can be seen that the simulations exhibit substantial seasonal variation compared with available observations. Both the ARW-MODIS and ARW-CRISP LULC datasets capture well the diurnal variation of AT. The ARW-MODIS simulations show cold bias, while the ARW-CRISP simulations exhibit some warm bias in all seasons except the FIMP. The highest mean AT is noticed during the FIMP (28.58°C) and the lowest in the NEMS (26.8°C). Day and night variation of AT is highest in the FIMP (9.0°C) and lowest in the NEMS (5.5°C). RH has an almost uniform pattern for all seasons, with the observed mean RH changing

TABLE 7 Statistical examination of rainfall (mm) with MODIS and CRISP

Errors	MODIS	CRISP
MB	21.70	−15.34
MAE	67.60	37.03
RMSE	91.42	46.25
CC	0.79	0.90

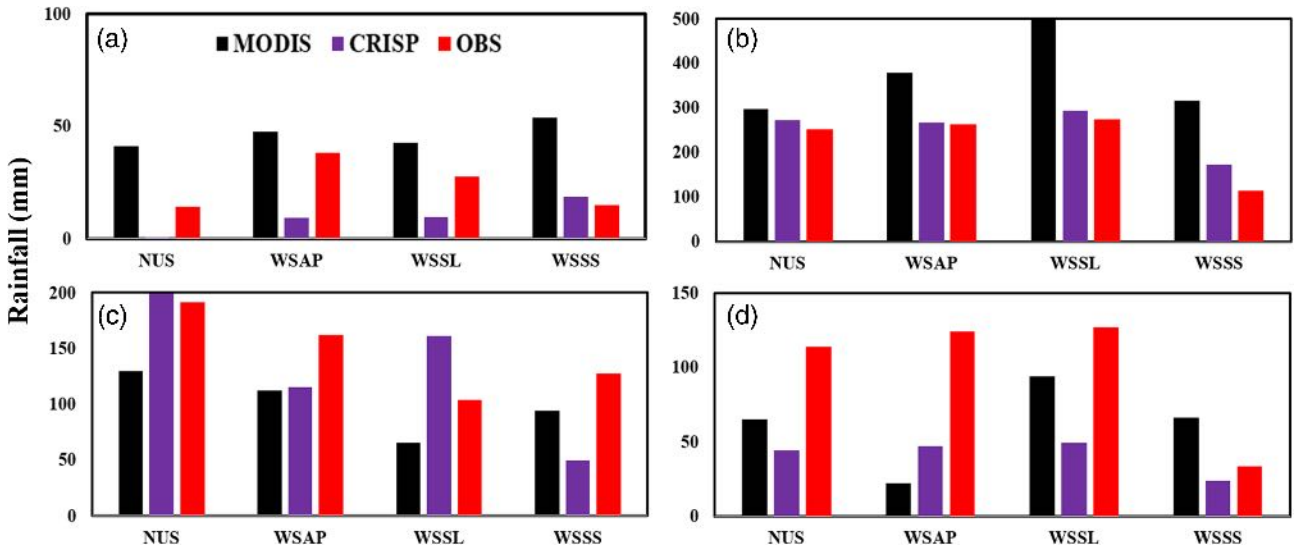

FIGURE 9 Validation of ARW model simulated seasonal accumulated rainfall (30 days) during (a) the northeast monsoon season, (b) the first inter-monsoon period, (c) the southwest monsoon season and (d) the second inter-monsoon period over the Singapore region with observations

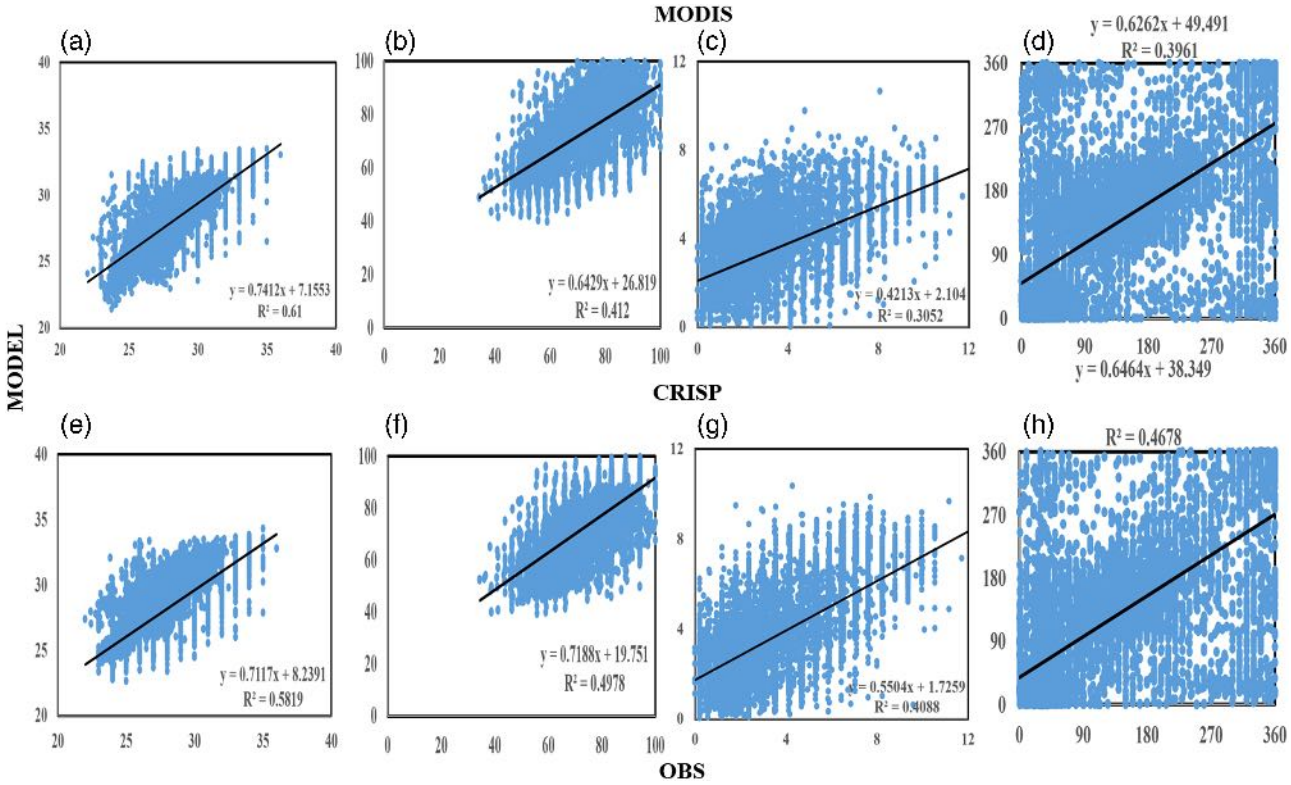

FIGURE 10 Scatter plot of ARW model simulated and observed surface air temperature (a), (e), wind speed (b), (f), relative humidity (c), (g) and wind direction (d), (h) for the study period

from around 73% to 76%. Both ARW-MODIS and ARW-CRISP simulations capture well the seasonal variation and diurnal variation of RH, but a slight overprediction is noticed for ARW-MODIS except for the SIMP and a slight underprediction for ARW-CRISP. In the case of RH, less error is noticed with the ARW-CRISP dataset compared to the ARW-MODIS dataset for all the seasons. In general, both WS and WD are well captured by the model (apart from WD in the FIMP and SIMP), with stronger prevalent winds in the monsoon seasons compared to the inter-monsoon periods (Tables 3–6). In general, WS is better simulated in inter-monsoon periods, while WD is better simulated in monsoon seasons. Overall, the use of the ARW-CRISP LULC dataset generally resulted in fewer errors than the use of the ARW-MODIS dataset for most surface meteorological variables (except AT) in all seasons.

4.2 | Accumulated rainfall

Atmospheric dispersion models and air quality models require many meteorological variables, such as PBL height, flow-field, atmospheric stability, AT, RH, rainfall and various other quantities. Accurate prediction of rainfall is one of the most difficult variables in NWP, and a lot of work has been aimed at improving numerical models for rainfall prediction during the past few decades (Wang and Seaman, 1997). Rainfall has a scavenging effect, as it washes particulate matter and dissolves gaseous pollutants from the atmosphere. In general, where high rainfall occurs frequently, air quality is better. The validation of ARW-MODIS and ARW-CRISP simulated seasonal accumulated rainfall (30 days) during all seasons (NEMS, FIMP, SWMS and SIMP) over Singapore is shown in Figure 9. The errors calculated between the model simulated and observed rainfall for the combination of all four observation stations and four seasons are shown in Table 7. Seasonal observed accumulated rainfall is the highest in the FIMP (898.6 mm) followed by the SWMS (548.8 mm), the SIMP (398.6 mm) and the NEMS (94.5 mm). The mean observed AT rainfall for the study period is 123.5 mm. Simulations with the ARW-MODIS and ARW-CRISP datasets fail to predict the rainfall in the NEMS. The ARW-MODIS simulations overestimate and the ARW-CRISP simulations underestimate the accumulated rainfall. However, the ARW-CRISP LULC dataset simulations show less error; a higher correlation is noticed and they are mostly closer to the observed rainfall, apart for a few cases.

4.3 | Statistical examination of surface meteorological variables

Scatter plots of model-simulated surface meteorological variables versus observations combining all seasons and all stations (Figure 10) reveal that the AT and RH are scattered whereas WS and WD are widely scattered. The results show that the thermodynamic variables are better simulated than the wind characteristics. The ARW-MODIS simulations result in somewhat better agreement (i.e. higher r^2) for AT, while the ARW-CRISP simulations show better results for RH, WS and WD (Figure 10). Thermodynamic variables will be significant to many processes involved with air pollution. For example, PBL development, which is strictly linked to surface fluxes, is one of the key points for air quality. In addition, secondary pollutants, such as ozone, will depend strongly on AT. Moisture will determine many processes related to particles in the air. For air quality and atmospheric chemistry studies, WS and WD are more critical than the thermodynamic quantities (Madala *et al*., 2016). Overall, the scatter plots indicate that the ARW model can replicate both surface meteorological variables over Singapore with somewhat higher accuracy using the ARW-CRISP LULC dataset than the standard ARW-MODIS dataset.

5 | SUMMARY AND CONCLUSIONS

In the present study, the performance of a regional Centre for Remote Imaging, Sensing and Processing (ARW-CRISP) land use land cover (LULC) dataset and the standard global ARW Moderate Resolution Imaging Spectroradiometer (ARW-MODIS) LULC dataset in an Advanced Research Weather Research and Forecasting (ARW) mesoscale model were compared simulating specific features of seasonal mesoscale atmospheric flow-field variables over the Singapore region. The simulated surface meteorological variables and rainfall are validated both qualitatively and quantitatively with available local observations. Overall, thermodynamic quantities (air temperature [AT] and relative humidity [RH]) were better simulated than wind characteristics. The highest mean AT and the highest day and night variation in the AT were noticed in the first inter-monsoon period (FIMP). The study found that RH has an almost uniform pattern for all seasons. The strongest surface wind speed (WS) was noticed in monsoon seasons compared to inter-monsoon periods. The surface WS was better simulated in inter-monsoon periods, while the wind direction (WD) was better simulated in the monsoon seasons. Seasonal accumulated rainfall during our observation periods was highest in the FIMP followed by the southwest monsoon season, the second inter-monsoon period and the northeast monsoon season. The results highlight strong seasonal variations of winds in Singapore, thereby emphasizing the importance of reliable WS and WD modelling for monitoring and predicting the dispersion of air pollutants in the region. In general, the regional land cover map produced in the ARW-CRISP dataset resulted in better simulations of surface meteorological variables and accumulated rainfall compared to the standard ARW-MODIS LULC dataset.

Somewhat better agreement with the field observations, particularly wind characteristics, was achieved with the regional ARW-CRISP map than the standard ARW-MODIS product. A significant difference of the two land cover datasets used in the present study was the year of acquisition of the underlying satellite data. The standard ARW-MODIS land cover dataset is based on 2001 satellite data, while the ARW-CRISP map was produced with 2015 data. In particular in areas which experience rapid land cover changes (like southeast Asia), use of up-to-date land cover information should be encouraged (Cheng *et al*., 2013; Schicker *et al*., 2015).

Overall, the study shows that flow-field variables and rainfall influence the dispersion of air pollutants and air quality differently in different seasons (Madala *et al*., 2015). A land cover product specifically developed for the conditions of this region enabled somewhat better simulation of these seasonal variations than a global land cover dataset. The results of the present study therefore advocate the use of regional LULC products in the ARW model for simulations of the planetary boundary layer flow-field variables for air quality assessment and prediction over the Singapore region. Overall, the present study indicates possibilities to improve regional level air quality monitoring and prediction capabilities over Singapore.

ACKNOWLEDGEMENT

The National Research Foundation, Prime Minister's Office, Singapore, under the Office for Space Technology and Industry Space Research Programme (project number S15-1319-NRF OSTIn-SRP) supports this research project. The authors express thanks anonymous reviewers for their technical comments and suggestions, which helped to improve the paper.

ORCID

Srikanth Madala https://orcid.org/0000-0003-2781-1586

REFERENCES

Banks, R.F. and Baldasano, J.M. (2016) Impact of WRF model PBL schemes on air quality simulations over Catalonia, Spain. *Science of the Total Environment*, 572, 98–113.

Banks, R.F., Tiana-Alsina, J., Baldasano, J.M., Rocadenbosch, F., Papayannis, A., Solomos, S. and Tzanis, C.G. (2016) Sensitivity of boundary-layer variables to PBL schemes in the WRF model based on surface meteorological observations, lidar, and radiosondes during the HygrA-CD campaign. *Atmospheric Research*, 176-177, 185–201.

Cheng, F.-Y., Hsu, Y.-C., Lin, P.-L. and Lin, T.-H. (2013) Investigation of the effects of different land use and land cover patterns on mesoscale meteorological simulations in the Taiwan area. *Journal of Applied Meteorology and Climatology*, 52(3), 570–587.

Chia, L.S. and Foong, S.F. (1991) Climate and weather. In: Chia, L.S., Rahman, A. and Tay, D.B.H. (Eds.) *The Biophysical Environment of Singapore*. Singapore: Singapore University Press and the Geography Teachers' Association of Singapore, pp. 13–49.

Friedl, M.A., McIver, D.K., Hodges, J.C.F., Zhang, X.Y., Muchoney, D., Strahler, A.H., Woodcock, C.E., Gopal, S., Schneider, A., Cooper, A., Baccini, A., Gao, F. and Schaaf, C. (2002) Global land cover mapping from MODIS: algorithms and early results. *Remote Sensing of Environment*, 83, 287–302.

Garcia-Diez, M., Fernandez, J., Fita, L. and Yague, C. (2013) Seasonal dependence of WRF model biases and sensitivity to PBL schemes over Europe. *Quarterly Journal of the Royal Meteorological Society*, 139, 501–514.

Hansen, M.C., Potapov, P.V., Moore, R., Hancher, M., Turubanova, S.A., Tyukavina, A., Thau, D., Stehman, S.V., Goetz, S.J., Loveland, T.R., Kommareddy, A., Egorov, A., Chini, L., Justice, C.O. and Townshend, J.R.G. (2013) High-resolution global maps of 21st-century forest cover change. *Science*, 342, 850–853.

Hu, X.-M., Nielsen-Gammon, J.W. and Zhang, F. (2010) Evaluation of three planetary boundary layer schemes in the WRF model. *Journal of Applied Meteorology and Climatology*, 49, 1831–1844.

Li, X.-X., Koh, T.-Y., Entekhabi, D., Roth, M., Panda, J. and Norford, L.K. (2013) A multi-resolution ensemble 125 study of a tropical urban environment and its interactions with the background regional atmosphere. *Journal of Geophysical Research – Atmospheres*, 118, 9804–9818.

Li, X.-X., Koh, T.-Y., Panda, J. and Norford, L.K. (2016) Impact of urbanization patterns on the local climate of a tropical city, Singapore: an ensemble study. *Journal of Geophysical Research – Atmospheres*, 121, 4386–4403.

Madala, S., Salinas, S.V., Wang, J. and Liew, S.C. (2019) Customization of the Advanced Research Weather Research and Forecasting model over the Singapore region: impact of planetary boundary layer schemes, land use, land cover and model horizontal grid resolution. *Meteorological Applications*, 26(2), 221–231. https://doi.org/10.1002/met.1755.

Madala, S., Satyanarayana, A.N. and Srinivas, C.V. (2017) Performance of WRF for simulation of mesoscale meteorological characteristics for air quality assessment over tropical Coastal City Chennai. *Pure and Applied Geophysics*, 175, 501–518. https://doi.org/10.1007/s00024-017-1662-3.

Madala, S., Satyanarayana, A.N.V., Srinivas, C.V. and Kumar, M. (2015) Mesoscale atmospheric flow-field simulations for air quality modeling over complex terrain region of Ranchi in eastern India using WRF. *Atmospheric Environment*, 107, 315–328.

Madala, S., Srinivas, C.V., Hariprasad, K.B.R.R. and Satyanarayana, A.N.V. (2016) Air quality simulation of NOX over the tropical coastal city Chennai in southern India with FLEXPART-WRF. *Atmospheric Environment*, 128, 65–81.

Miettinen, J., Shi, C. and Liew, S.C. (2016) 2015 land cover map of Southeast Asia in 250 m spatial resolution. *Remote Sensing Letters*, 7, 701–710.

Preeti, G. and Manju, M. (2017) Sensitivity of WRF model estimates to various PBL parameterizations in different climatic zones over India. *Atmospheric Research*, 194, 43–65.

Rafee, S., Kawashima, A., Morais, M., Urbina, V., Martins, L. and Martins, J. (2015) Assessing the impact of using different land cover classification in regional modeling studies for the Manaus area Brazil. *Journal of Geoscience and Environment Protection*, 3, 77–82.

Schicker, I., Arnold, A.D. and Seibert, P. (2015) Influences of updated land-use datasets on WRF simulations for two Austrian regions. *Meteorology and Atmospheric Physics*, 128, 1–23. https://doi.org/10.1007/s00703-015-0416-y.

Singh, J., Yeo, K., Liu, X., Hosseini, R. and Kalagnanam, J.R. (2015) Evaluation of WRF model seasonal forecasts for tropical region of Singapore. *Advances in Science and Research*, 12, 69–72.

Skamarock, W. C., Klemp, J. B., Dudhia, J., Gill, D. O., Barker, D. M., Dudha, M. G., Huang, X., Wang, W., Powers, Y., 2008. A Description of the Advanced Research WRF Ver.30. In: NCAR Technical Note. NCAR/TN-475STR. Meso-scale and Micro-scale Meteorology Divison, National Centre for Atmospheric Research, Boulder Colorado, USA, 113 pp

Stull, R.B. (1988) *Introduction to Boundary Layer Meteorology, xiii + 666 pp. Dordrecht*. Boston; London: Kluwer Academic Publishers.

Tao, Z., Santanello, J.A., Chin, M., Zhou, S., Tan, Q., Kemp, E.M. and Peters-Lidard, C.D. (2013) Effect of land cover on atmospheric processes and air quality over the continental United States – a NASA unified WRF (NU-WRF) model study. *Atmospheric Chemistry and Physics*, 13, 6207–6226.

Tyagi, B., Satyanarayana, A.N.V., Kumar, M. and Mahanti, N.C. (2012) Surface energy and radiation budget over a tropical station: an observational study. Asia Pac. *Journal of the Atmospheric Sciences*, 48(4), 411–421.

Wang, W. and Seaman, N.L. (1997) A comparison of convective parameterization schemes in a mesoscale model. *Monthly Weather Review*, 125, 252–278.

Yang, J. and Duan, K. (2016) Effects of initial drivers and land use on WRF modeling for near-surface fields and atmospheric boundary layer over the Northeastern Tibetan Plateau. *Advances in Meteorology*, 2016, 7849249, 16. https://doi.org/10.1155/2016/7849249.

SUPPORTING INFORMATION

Additional supporting information may be found online in the Supporting Information section at the end of this article.

How to cite this article: Madala S, Salinas SV, Miettinen J, Wang J. Numerical simulation of seasonal mesoscale atmospheric flow-field variables using ARW over the Singapore region: impact of land use land cover. *Meteorol Appl*. 2020;27:e1846. https://doi.org/10.1002/met.1846